High-pressure structural systematics of dysprosium metal compressed in a neon pressure medium to 182 GPa

D. T. Sneed,[1,*] P. Söderlind,[1] E. F. O'Bannon, III,[1] H. Cynn,[1] D. Smith,[2,3] J. S. Smith,[2] C. Park,[2] and Zs. Jenei[1]

[1]*Physics Division, Physical and Life Sciences Directorate, Lawrence Livermore National Laboratory, Livermore, California 94550, USA*
[2]*High Pressure Collaborative Access Team, X-Ray Science Division, Argonne National Laboratory, Argonne, Illinois 60439, USA*
[3]*Nevada Extreme Conditions Laboratory, University of Nevada, Las Vegas, Las Vegas, Nevada 89154, USA*

(Received 11 March 2022; revised 18 May 2022; accepted 24 May 2022; published 23 June 2022)

We present an experimental and theoretical study of dysprosium metal compressed in the soft pressure transmitting medium Ne up to 182 and 300 GPa, respectively. Angle-dispersive x-ray powder diffraction data from each of the high-pressure polymorphs shows anisotropic compression behavior indicating changes to the electron density distribution throughout its polymorphic landscape. We compare the monoclinic (*m*C4) and orthorhombic (*o*F16) structures for the collapsed structure for Dy above 82 GPa and verify that the *o*F16 structure offers a better fit to our data than the previously reported *m*C4 structure. Further, we have found that the *o*F16 structure undergoes similar anisotropic compression of its lattice parameters, with a turning point above 160 GPa; suggesting a potential phase transition at pressures much higher than achieved in this study. Density functional theory calculations show the likely candidate for this new high-pressure phase is the isosymmetric *o*F8 structure, which is predicted to be lower in energy than the *o*F16 structure above 275 GPa.

DOI: 10.1103/PhysRevB.105.214110

I. INTRODUCTION

The behavior of $4f$-shell rare-earth metals under extreme conditions is of great interest due to the pressure mediated hybridization of the *spd* orbitals which creates anomalous structural behaviors and unique electronic and magnetic properties [1]. The appearance of low-symmetry crystal structures with an accompanying volume collapse under high pressures in lanthanide systems is generally attributed to a delocalization of the f-orbital electrons. As pressure is increased, *spd* hybridization occurs allowing new crystalline structures to become energetically stable [1,2], until the energetics of the system drive the f electrons to enter an itinerant state [2,3]. Once the f electrons become itinerant, it has been discussed that they begin to participate in metallic bonding, facilitating a volume collapse into a lower symmetry structure [2,4]. Though it is widely accepted that the volume collapse in f-electron systems is due primarily to the delocalization of the f electrons [3], experiments using x-ray absorption spectroscopy and x-ray emission spectroscopy show very little change to the f electrons across the pressure region of the volume collapse transition in Gd and Tb, while there is a strong signature of $s \rightarrow d$ electron transfer [5]. This suggests that the Kondo resonance mitigated volume collapse in f-electron systems could in fact be driven more by the *spd* hybridization than an itinerant f-electron state. This would also explain the strong similarities between the polymorphism seen in the d-block element Y and what is seen in the heavy lanthanides [6]. In the light rare-earth metals Ce, Pr, and Nd, crystal structures such as body centered tetragonal (bct) [7], α-uranium [8], and orthorhombic *o*F8 [9] have been observed under high pressures, respectively. Similarly, the heavy rare-earth metals have been shown to undergo a volume collapse into the low-symmetry monoclinic *m*C4 structure; however, recently, McMahon *et al.* [4] have shown that the collapsed phase was more likely the orthorhombic *o*F16 structure. These lower symmetry structures indicate the participation of f electrons in metallic bonding, though the mechanism of this transition is still the subject of much interest [10,11].

Dy is a trivalent rare-earth metal which has an ambient pressure electronic configuration with three electrons in the *spd* conduction band and nine electrons in the localized $4f$ shell [12] and crystallizes under ambient conditions in a hexagonal close-packed (hcp) structure with space group $P6_3/mmc$. The application of pressure is expected to cause *spd* hybridization, much like that which has been observed in other lanthanides as well as lighter elements [5,13]. At sufficiently high pressure there is a volume collapse into a lower symmetry phase, as in other lanthanides [5,14,15]. Previous studies of Dy have shown it to follow the typical rare-earth structural sequence through the distorted face-centered cubic (dfcc) phase: hcp→α-Sm type, α-Sm type→dhcp (dhcp is double hexagonal-close-packed), and dhcp→dfcc (*h*P2 → *h*R9 → *h*P4 → *h*R24 in Pearson notation) [12,16–19]; however, there is some discrepancy in the transition pressures reported throughout the literature, which will be discussed in this paper.

Most of the experiments on the lanthanides at ultrahigh pressures reported in the literature were performed under nonhydrostatic conditions, and specifically for the case of Dy, experiments were performed either with no pressure transmitting medium [12,18,19], with silicon oil [16], or methanol/ethanol [17]. Nonhydrostatic conditions can cause complex stress fields, deviatoric stress, and complex phase

*sneed2@llnl.gov

behavior upon compression [20]. Anisotropic stress fields on the sample can lead to the appearance of metastable phases that may not exist when the sample is compressed under more hydrostatic conditions [21]. Furthermore, the majority of these studies, with the exception of Tschauner *et al.* [17] and Hope *et al.* [18], give no discussion of the behavior of the lattice parameters with pressure. In the present work, we perform a detailed analysis of Dy metal compressed in a soft, quasihydrostatic Ne pressure medium with the goal of gaining a better understanding of the complex structural response of Dy under compression. We examine lattice parameter response, the axial ratios, and the pressure-volume relations of each of the high-pressure polymorphs of Dy up to 182 GPa and discuss how the pressure/volume response deviates when under nonhydrostatic compression. We also apply density functional theory (DFT) to both study the lattice parameter response of the collapsed phase, and to compare the relative energies of multiple structures to explore the possibility of new high-pressure phases.

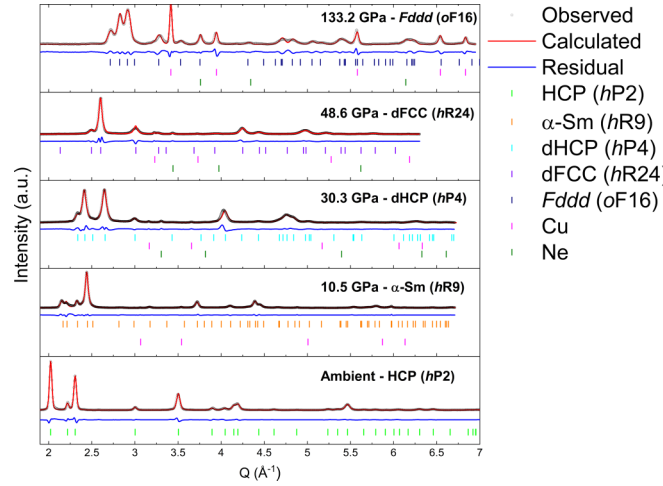

FIG. 1. Representative Le Bail refinements from each phase of Dy up through the collapsed phase.

II. METHODS

A. Experiment

We present three experimental runs on Dy to different maximum pressure conditions using membrane diamond-anvil cells (DACs) [22]. For the first experiment, diamonds with a 500-μm culet size were used and a maximum pressure of $\sim$10 GPa was achieved. A hole diameter of $\sim$180 μm was drilled using electron discharge machining into a Re gasket preindented to a thickness $\sim$30 μm. For the second and third experiments, diamonds with 100-/300-μm beveled culets were used, and a hole diameter of $\sim$60 μm was drilled into a Re gasket preindented to a thickness $\sim$25 μm. Maximum pressure achieved in the last two runs was $\sim$51 and $\sim$182 GPa, respectively. A Dy metal ingot (Alfa Aesar, 99.9%) was handled under a dry nitrogen atmosphere, and samples were obtained by scraping the ingot surface down approximately 100 μm, exposing pure metal. A small piece of oxide-free sample was selected carefully and loaded, along with Cu powder (Alfa Aesar, 99.9%) and a small ($\sim$5 μm) ruby sphere. The Cu was loaded into the sample chamber in such a way to ensure the x-ray beam would pass through both the sample and the pressure marker. The DACs were closed in the dry nitrogen atmosphere to prevent oxidation of the Dy sample prior to Ne gas loading. To further ensure that no oxygen contamination was introduced during gas loading, the high-pressure chamber of the gas loader was evacuated with a vacuum pump prior to pressurizing the chamber with 99.999% pure Ne to $\sim$0.18 GPa. The cell was opened to allow the Ne to enter the chamber and then closed and brought to a pressure of $\sim$1 GPa, verified using the calibrated ruby fluorescence shift [23]. For ambient measurement, sample was loaded into a cell employing 750-μm culets and a stainless-steel gasket. One piece of the sample was carefully selected and placed in the gasket hole using the same methods described above; the cell was closed to ensure the sample chamber was sealed, but no pressure was applied to the sample. Full pattern refinement of ambient data using a space group of $P6_3/mmc$ gives lattice parameters $a = 3.5869(4)$ Å and $c = 5.665(1)$ Å (see Ref. [24]).

Angle-dispersive x-ray diffraction experiments were carried out at the Advanced Photon Source (APS) High-Pressure Collaboration Access Team (HPCAT) beamline 16 BM-D. A monochromatic x-ray beam of 25.0 keV ($\lambda = 0.4959$ Å) was focused to a beam size of $\sim 4\times4$ μm^2 full width half maximum with $\sim 16\times16$ μm^2 tails at less than 1% max. Diffraction patterns were collected with a MAR-345 image plate detector with exposure times up to 120 s. X-ray diffraction was also performed at the 16 ID-B diffraction beamline with a monochromatic x-ray energy of 30.5 keV ($\lambda = 0.4066$ Å), beam size of $\sim 1\times2$ μm^2, and a Pilatus1M Si detector with exposure times up to 60 s. Sample positioning and centering was accomplished by the fly scan method [25]. Detector distance and orientation was calibrated using a CeO_2 standard for both beamlines. c-BN backing plates were used on the downstream side of the cell in each experiment, ensuring full 2θ coverage up to a minimum q of 6 Å^{-1}. Initial x-ray diffraction grid scans of sample compartments in each experiment indicated that the Dy samples were pure, and no oxide was observed in the patterns.

Two-dimensional diffraction images were integrated into one-dimensional patterns using the DIOPTAS software package [26]. One-dimensional diffraction patterns were analyzed to obtain peak positions using our in-house analysis codes in the ORIGINPRO software package. Dy volumes were calculated directly from fitted peak positions and compared to full pattern refinements at various pressures using GSAS-II [27] and comparisons between the two methods are shown for the collapsed phase in Ref. [24]. Representative two-dimensional patterns for each phase and corresponding full pattern refinements are shown in Fig. 1 and refinement results are listed in Ref. [24]. Intensities were not refined, therefore atomic positions listed in Ref. [24] are for reference only and are taken from Refs. [4,12,16].

The sample pressure was estimated by measuring the unit cell volume of Cu and Ne using the (111) reflection and the equations of state (EOS) reported by [28,29], respectively. Pressure uncertainties were determined by propagating the reported uncertainties in the bulk modulus and the first pressure derivative from the reported equation of states, uncertainties

from peak fits, and the difference in pressures calculated from Ne and Cu. All pressure, volume, and lattice parameter values measured in these experiments are listed in Ref. [24]. Equation of state fitting was performed on all data using EoSFit7-GUI [30], and the fit results are listed in Ref. [24].

B. Theoretical

A good approach for modeling phase stability and equation of state for materials under compression is that of density functional theory. Generally, it works very well and errors in the predictions tend to decrease with pressure [31]. The rare-earth metals are more challenging to model than most other metals because strong electron-correlation effects localize the $4f$ electrons at ambient condition. Often such localization effects are modeled within the DFT+U approach where a Hubbard U parameter is introduced to address a large intra-atomic Coulomb repulsion that is neglected in conventional DFT. This approach, however, has shown to fail in addressing the high-pressure behavior of rare-earth metals [32]. Instead, we improve on DFT with an extension that involves the otherwise absent orbital-orbital interaction in an orbital polarization (OP) scheme. This orbital polarization phenomenon is related to Hund's second rule for the atoms and attempts to bring some atomic physics into the DFT model. It has been shown that DFT+OP can relatively accurately reproduce known bonding properties such as lattice constants and bulk modulus as well as magnetic properties for the rare-earth metals [33]. DFT+OP has also successfully been applied for high-pressure studies of the rare-earth metal Pr [34].

For high-pressure conditions, where one expects delocalization of the $4f$ electrons, DFT+OP is a sensible technique to study equation of state and crystal-structure stability. We employ an all-electron full potential linear muffin-tin orbitals method [35] that includes spin-orbit coupling and assumes the generalized gradient approximation (GGA) for the electron exchange and correlation functional. Details of the calculations are similar to those we have performed previously for the rare-earth metals [33] that also show GGA is superior to the local-density approximation for Pr. Briefly, the setup includes $5s$, $5p$, $6s$, $6p$, $5d$, and $4f$ states that have two energy parameters associated with them for a so-called double basis set. Spin-orbit coupling and orbital polarization are included for the d and f states only and the overall computational scheme is entirely free from adjustable parameters.

III. RESULTS AND DISCUSSION

A. Structural systematics up to 80 GPa

We started our high-pressure experiments at ∼1.7 GPa with the sample in the hcp (hP2) phase and observed anisotropic compression behavior in which the c axis begins as being more compressible than the a axis. The c/a ratio decreases by about 0.5% before reaching a turning point at ∼3.5 GPa shown in Fig. 2(a). After this inflection, the c/a ratio increases by about 1.5% until it reaches a maximum above 5.8 GPa, and above this pressure reflections from the α-Sm type phase begin to appear. We attempted to fit a "global" EOS to the P-V data up to 82 GPa (just before the volume collapse transition happens), an approach similar to those reported in previous studies [12,18,19]. However, we found that a third- or fourth-order EOS could not adequately fit the P-V data, and this global fit did not capture the differences in compressibility of each phase. Therefore, we fit each phase separately with a fully weighted third-order (or fourth order in the case of the dfcc phase) Birch-Murnaghan EOS [30,36,37]. For the hcp phase we fixed V_0 to 31.562(7) Å^3, which was determined from our ambient measurement, and obtained a bulk modulus of $B_0 = 45.3(3)$ GPa and its pressure derivative $B'_0 = 0.72(8)$. Figure 3 shows the bulk modulus as a function of pressure calculated directly from the P-V data using $-V(\frac{\partial P}{\partial V})_T$ and calculated using the EOS parameters determined from our fit [30]. When examining the bulk modulus as a function of pressure for the hcp phase [shown in better detail in Fig. 3(b)], there appears to be a softening of ∼5% which correlates to the anisotropic behavior of c/a leading up to the transition to α-Sm type. Above 6.5 GPa, hcp peaks could no longer be fully resolved, and α-Sm was the only phase present. This behavior in the hcp phase of Dy was also reported by Tschauner *et al.* [17]. In their work, they showed a marked reduction in the c/a ratio caused by anisotropic compressibility of the a and c axes followed by an inflection point at ∼2.5 GPa. There is a difference of ∼1 GPa in the location of the apparent inflection point in Ref. [17] and in our experiment; however, there is good agreement between the relative behavior of two experiments within the error bars (see Ref. [24]). This difference in pressure measured for the inflection point may be a result of differences in data density between our experiment and that of Ref. [17].

The mechanism which drives this anisotropy in the compression behavior of the hcp lattice parameters has been thoroughly discussed in [17] and has been attributed to an isostructural topological transition driven by $s \rightarrow d$ orbital hybridization. This $s \rightarrow d$ hybridization drives a shift in the electron density distribution within the ab plane. As electron density near the Fermi level increases, Coulomb repulsion drives the electron density further from the central atoms within the ab plane while the electron density within the c axis remains localized to the central atoms. The turning point occurs when the electron density within the ab plane becomes distributed to a point in which the Coulomb repulsion between atoms lowers, leading to a softening of the ab plane and a subsequent stiffening of the c axis. This is made evident by the inflections of normalized lattice parameters above 3.5 GPa shown in Fig. 2(a). Interestingly, values reported by Hope *et al.* [18] do not clearly show this inflection point; in fact, their c/a ratio appears to continuously decrease through the α-Sm phase. The deviation of [18] from this trend seen in both our experiment and that of [17] is most likely due to nonhydrostatic conditions.

The α-Sm phase also exhibits anisotropic compression in which the c/a ratio increases by ∼2% leading up to an inflection point (similar to that of the hcp phase), which occurs at 13 GPa, following a slight distortion to the c axis. After this inflection point, the c/a ratio decreases by ∼1% until the dhcp phase begins to appear above 17 GPa, after which the c/a ratio becomes nearly linear indicating isotropic compressibility between the a and c axes [see Fig. 2(b)]. Fitting an EOS to the P-V data from 6 to 17 GPa (the α-Sm stability region), we found that B_0 decreases from that of the hcp phase to

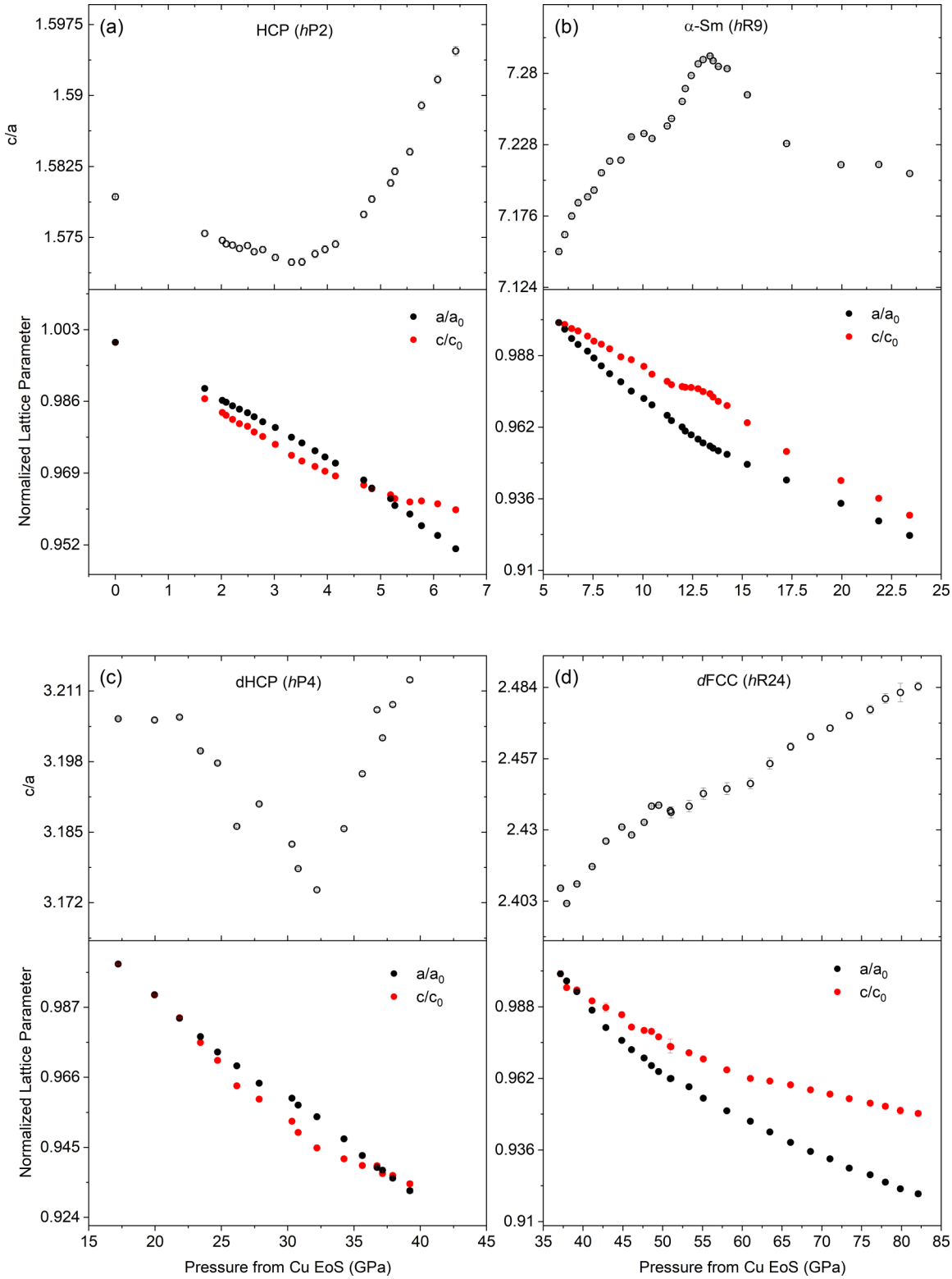

FIG. 2. Normalized lattice parameters along with the c/a ratio showing the changes in relative compressibility of the different axis of the hexagonal basis symmetry polymorphs (a) hcp (*h*P2), (b) α-Sm (*h*R9), (c) dhcp (*h*P4), and (d) dfcc (*h*R24). Each structure shows anisotropic behavior with pressure along with turning points in the c/a ratio which has been attributed to a topological phase transition in the hcp structure [17].

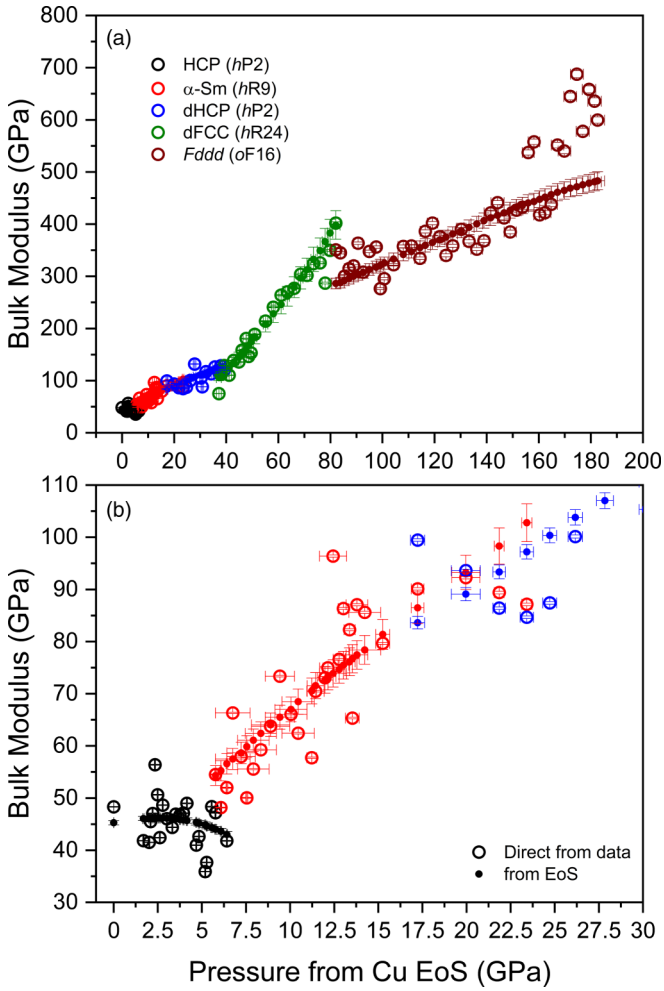

FIG. 3. (a) Isothermal bulk modulus as a function of pressure calculated directly from the data (hollow circles) and best fit using Birch-Murnaghan EOS (solid circles) across the entire pressure range of our measurements. (b) Low-pressure region up to 30 GPa showing the trend in the bulk modulus for the hcp phase of Dy.

36.2(7) GPa and B′$_0$ increases to 3.4(1). We did attempt to fit V_0 for the α-Sm phase but found a fit value which was nearly identical to that of the measured ambient data; thus, given the continuous nature of the hcp→α-Sm transition, we fixed V_0 to the ambient value. We found α-Sm to be the stable phase up to 17.5 GPa, at which point reflections from the dhcp phase appear and the relative intensities of the reflections from the α-Sm phase begin to decrease. This continues until reflections from the α-Sm phase disappear completely above 23.5 GPa, after which only reflections from dhcp Dy are observed. In the mixed phase region from ∼17.5 to 23 GPa the relative compressibilities of the a and c axes are nearly identical for both phases. Above 23 GPa, where pure phase dhcp is observed, there is a contraction of the c axis leading up to another turning point in the compression ratio near ∼32 GPa; above this pressure the c axis becomes less compressible, as shown in Fig. 2(c). There is a near continuous increase in bulk modulus starting above 6 GPa where the α-Sm phase becomes stable through the dhcp phase shown in Fig. 3. Fitting an equation of state to the P-V data from 23 to 37 GPa (the dhcp stability region), we obtained the parameters $B_0 = 37.5(4)$ GPa and $B_0' = 3.19(3)$, which are similar to values obtained for the α-Sm phase. V_0 was fixed to the ambient value for the same reason as discussed above. Upon further compression of the sample the dhcp phase begins to transition to the dfcc phase above 37 GPa, and this transition completes by 39 GPa. We did not observe an fcc phase which has been reported to be stable in other lanthanides [38] and postulated by Patterson *et al.* [12] to be stable between 37 and 43 GPa.

Regarding the structure of the dfcc phase, we found the *h*R24 structure, and not the proposed *o*S8 structure [16], best fits our observations agreeing with the previous studies of [12,18,19,39]. We found that a third-order Birch-Murnaghan EOS was unable to adequately fit the curvature in the dfcc phase, and we recognized that there was a quadratic form to the normalized pressure (F) vs Eulerian strain (f_E), shown in Ref. [24]. Therefore, we used a fourth-order Birch-Murnaghan EOS [30] to fit the P-V data from 39 to 82 GPa where the dfcc phase is stable and obtained the parameters $B_0 = 68(1)$ GPa, $B_0' = 0.7(2)$, and $B_0'' = 0.071(1)$ GPa^{-1}. V_0 was held fixed to the ambient value for the same reasons as discussed previously. The value of B_0 is notably higher than the previous phases leading a very steep slope of the bulk modulus as a function of pressure shown in Fig. 3. There is a discontinuity in bulk modulus vs pressure between the dhcp and dfcc phases in which dfcc starts at a compressibility of ∼20 GPa lower than that of the dhcp phase at 37 GPa, but it sharply increases to nearly 400 GPa by 82 GPa where we observe the volume collapse transition. There does not appear to be a clear turning point in the c/a ratio in the dfcc structure; however, there is a marked stiffening of the c axis above 55 GPa as shown in Fig. 2(d). Interestingly, this stiffening does correlate with a turning point in the normalized pressure (F) vs Eulerian strain (f_E), as well as correlates to where the scaled c/a ratio crosses the ideal value for a close-packed hexagonal lattice of 1.63 shown in Ref. [24].

B. Volume collapse transition

Upon further compression, the dfcc phase is followed by a lower symmetry phase that has a characteristic volume collapse associated with f-electron delocalization. We have measured the volume collapse transition at 82.1(1.6) GPa; however, there has been some discrepancy in the literature regarding this transition. Samudrala and Vohra [19] shows the volume collapse transition to occur above 82 GPa, which agrees well with the transition pressure determined in this study. Patterson *et al.* [12] found the collapse to occur above 73 GPa; however, the data density in the region around the volume collapse shown on their P-V plot is low and there is a large gap between the last data point in which the dfcc phase was measured at ∼69 GPa, and the first data point in the collapsed phase at ∼82 GPa. Shen *et al.* [16] shows the dfcc phase to remain stable up to 87 GPa, which is the highest pressure reached in their data. We predicate that they saw pure dfcc still at 87 GPa likely because they used silicone oil as a pressure transmitting medium and nonhydrostatic conditions may have stabilized this phase to that pressure. The standard deviation in pressure determined from multiple ruby spheres loaded in silicone oil shows that above ∼2.5 GPa silicone

oil is nonhydrostatic [20]. Under nonhydrostatic conditions, measured volumes are larger than when they are measured under hydrostatic conditions [21]. Furthermore, they used ruby fluorescence calibrated from Holzapfel's 2003 refined ruby scale [22] to determine pressures throughout their experiment, which has been shown to overestimate pressure by up to 5 GPa at 100 GPa when compared to [23]. The effects of these can be seen when comparing their *P-V* data to other data sets on Dy (see Ref. [24]). Most recently, Hope *et al.* [18] show Dy compressed without a pressure medium up to a maximum pressure of 202 GPa. They find the transition to the collapsed phase to occur above 73 GPa, similar to what is seen in [12]. It should be noted that Hope *et al.* [18] list Cu EOS parameters of $B_0 = 121.6$ GPa and $B_0' = 5.583$; however, these parameters are ∼9% lower and ∼5% higher, respectively, than the Cu EOS parameters used in this study (see Ref. [28], Table II, *P* scale: P_R'). Choosing our reported Cu volume at the Dy volume collapse transition of 8.814 Å^3/atom, we calculate a pressure of 82.1 GPa using EOS parameters from [28] using a Vinet EOS vs a pressure of 80.3 GPa (or a difference of ∼2.2%) using the EOS parameters given in [18] calculated using a third-order Birch-Murnaghan EOS. As Hope *et al.* [18] did not report the V_0 they used for their Cu EOS, we used the value of 11.810 Å^3 reported in [28] for this comparison. This difference in EOS parameters cannot entirely explain the lower transition pressure reported for the volume collapse in [18]. However, it is known that nonhydrostatic conditions can reduce the transition pressure of a material and bias the obtained EOS parameters [20]. Therefore, the nearly 10 GPa difference in pressure measured for the volume collapse transition between this work and that of [18] is most likely due to a combination of nonhydrostatic conditions and the underestimation of pressure introduced by the EOS parameters used to calculate pressure in [18].

The initial structure solution for the collapsed phase was reported to be a monoclinic structure with four atoms per unit cell (*m*C4) with space group *C2/m* [4,12,19]. However, recently McMahon *et al.* [4] proposed the collapsed structure was in fact an orthorhombic structure with 16 atoms per unit cell (*o*F16) and space group *Fddd*. Their work showed that the collapsed phase of Tb, Gd, Dy, Ho, Er, and Tm is best modeled using the *o*F16 structure which showed a better fit to the observations than the *m*C4 structure (see Supplemental Material of Ref. [4]). To verify the *o*F16 structure also offered a better solution to the collapsed phase in our data, we performed a Le Bail refinement on the diffraction pattern collected at 134.7 GPa and found the *o*F16 structure to give a better solution than the *m*C4 structure, shown in Fig. 4. The fit residual was only marginally better with *o*F16 ($w_R = 1.25\%$ compared to $w_R = 1.35\%$ for *o*F16 and *m*C4, respectively), but the *m*C4 structural model could not account for a doublet located at $q \sim 5.25$ Å^{-1}, which was the same observation made in previous studies [4,18] and an in-depth discussion of the validity of the *o*F16 structure in the heavy lanthanides can be found in Ref. [4]. Hope *et al.* [18] also revisited the collapsed phase in Dy and showed that *o*F16 was indeed a better structural solution than the previously proposed *m*C4 structure.

There is also a large discrepancy in the literature on the magnitude of the volume collapse in Dy. Patterson *et al.* [12] measures a 6% volume collapse using the *m*C4 structure to describe the collapsed phase, whereas Samudrala and Vohra [19] report a 1.5% volume collapse using the same structure to describe the collapsed phase. Recently, Hope *et al.* [18] have reported a volume collapse of 2.3% using the *o*F16 structure to describe the collapsed phase. This wide variation in the degree of volume change in the dfcc→collapsed phase could be a direct result of the nonhydrostatic conditions present in each of these studies. In our study using a soft pressure transmitting medium we measure a 3.4(7)% volume collapse between the *h*R24 and *o*F16 phases, shown in Fig. 5(a). Fitting a third-order Birch-Murnaghan equation of state to the *P-V* data above 82 GPa where the *o*F16 phase is stable, we obtained $V_0 = 25.8(7)$ Å^3, $B_0 = 64(2)$ GPa, and $B_0' = 3.47(6)$. The fit begins to deviate from the data above 160 GPa [shown in Fig. 5(b) and Ref. [24]] as well as a large deviation of the bulk modulus calculated directly from the data and the bulk modulus calculated using the parameters determined from the EOS fit (shown in Fig. 3), suggesting a change in the

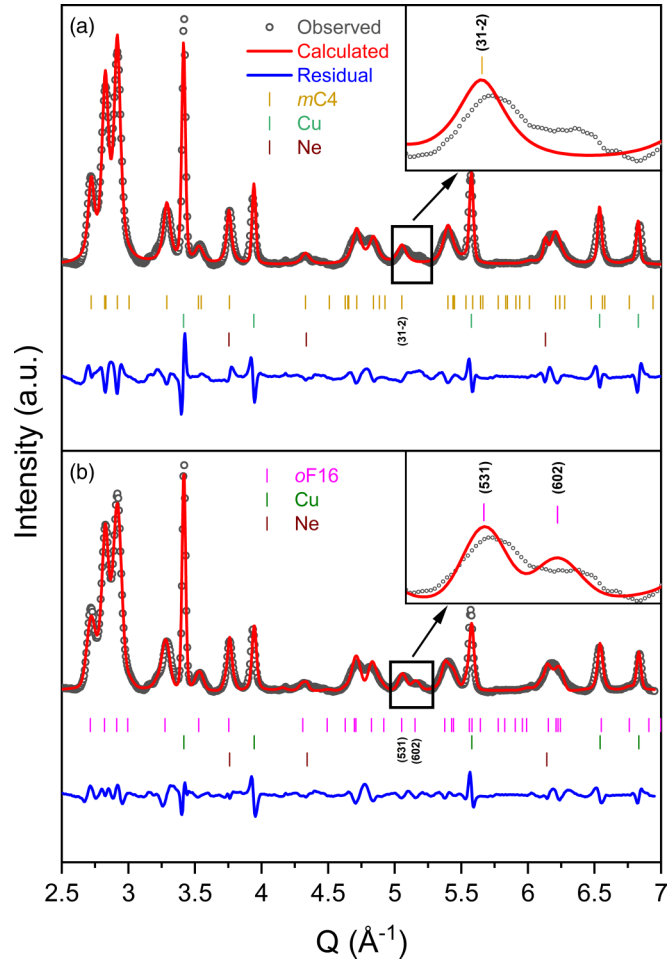

FIG. 4. Full pattern Le Bail refinements on the collapsed phase of Dy collected at 135 GPa comparing both the previously reported monoclinic *m*C4 structure (a) and the proposed orthorhombic *o*F16 structure (b). The predicted reflections for each structure are plotted beneath each pattern, orange being for the monoclinic structure and pink being for the orthorhombic structure. The two structures are very similar, but there is a clear splitting near 5.25 Å^{-1} shown in the insets which cannot be accounted for by the monoclinic structure.

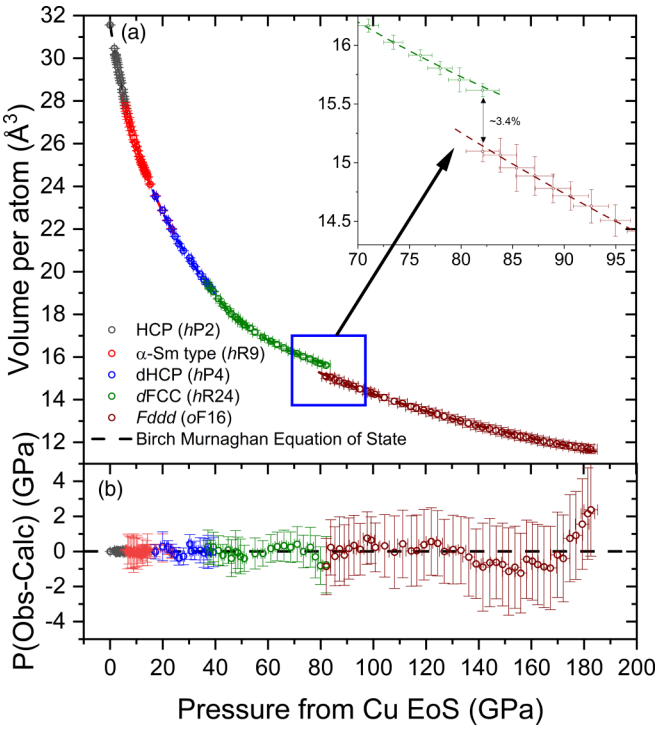

FIG. 5. (a) Volume per atom as a function of pressure for Dy across showing all polymorphs up to 185 GPa. The hollow symbols are data, the dashed lines are fits to a Birch-Murnaghan equation of state and (b) the difference between pressure calculated from the EOS fit and from the data. The inset shows an ∼3.4% volume collapse between *h*R24 and *o*F16 polymorphs when compressed in Ne.

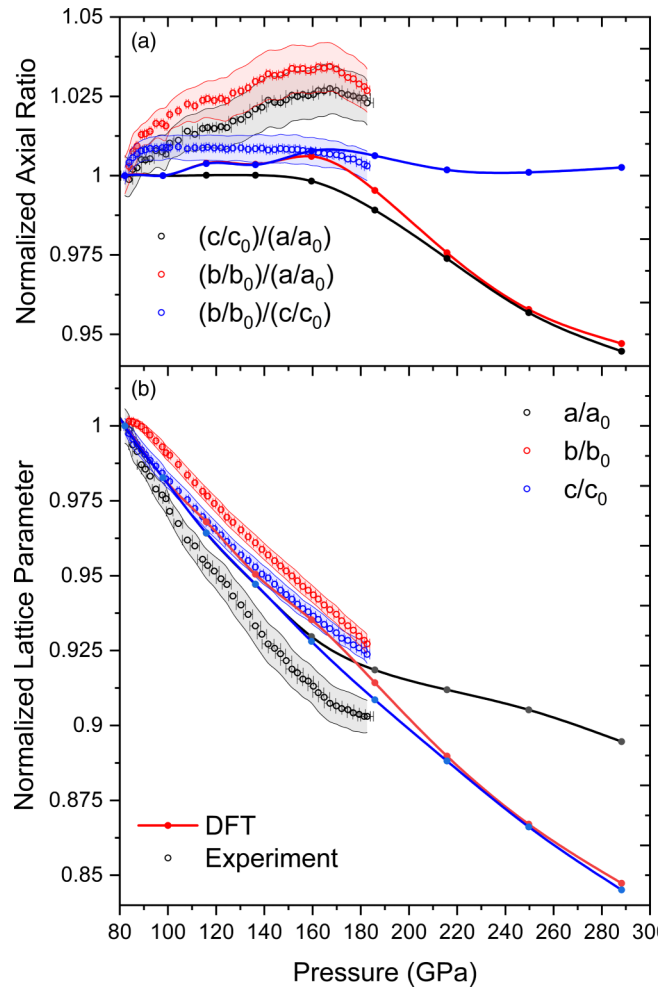

FIG. 6. Experimental data plotted with values determined from DFT comparing (a) normalized axial compression ratios and (b) normalized lattice parameters. Though there is an offset, DFT captures the turning points in axial ratios as well as the stiffening of the *a* axis above 160 GPa.

compressibility in the sample which the EOS cannot account for. Our V_0 is in good agreement with what was reported by Hope *et al.* [18] of $V_0 = 25.792$ Å^3; however, their value for $B_0 = 57.5$ GPa and $B'_0 = 3.59$ deviate from the values determined in this study. Their reported bulk modulus is ∼11% lower and their first pressure derivative is 3.3% higher than what we determined in this study. This deviation can be seen in their volumes lying ∼1.5% below the volumes determined in this study at 100 GPa (see Ref. [24]), which is most likely due to a combination of nonhydrostatic conditions, and the underestimation of pressure discussed previously.

C. Structural systematics beyond the volume collapse transition

The normalized lattice parameters along with the axial ratios for the orthorhombic phase are plotted along with calculated values in Fig. 6. A discussion on the uncertainties shown for the collapsed phase can be found in Ref. [24]. There is a clear turning point in each of the axial ratios, in which there is a stiffening of both the *a* and *c* axes above ∼160 GPa. This turning point in relative compressibility of the different lattice parameters is similar to what was observed in the lower pressure phases, which we interpret to be a result of changes in the electron density distribution and an indication of a possible phase transformation at much higher pressures. To explore this possibility, we performed DFT calculations for the collapsed orthorhombic phase and saw strong agreement between the experimental and theoretical values determined for the different lattice parameters, shown in Fig. 6. We then calculated the relative energies of multiple potential structures up to ∼300 GPa and found that the isosymmetric *o*F8 structure becomes the more energetically favorable structure, indicating a potential polytypic phase transition from *o*F16 to *o*F8 above 275 GPa (see Fig. 7). The primary difference between the two structures is a change in packing density with stacking arrangement shifting from an eight-layer BACBDCAD stacking to a four-layer ABCD stacking shown visually in Fig. 8. The four-layered *o*F8 structure has also been found to exist in Am between 10 and 17 GPa [40], in Cm between 56 and 96 GPa [41], and in Cf above 40 GPa [42]. For californium, the phase was predicted by DFT years before it was experimentally discovered (see discussion in [43]). In the case of Cm, the *o*F8 structure follows a continuous transition from a monoclinic structure with space group *C*2/*c*, which is similar to the previously accepted structure of the collapsed phase of the heavy lanthanides [41]. Figure 7 also shows that the slope of the energy of the bcc structure becomes very

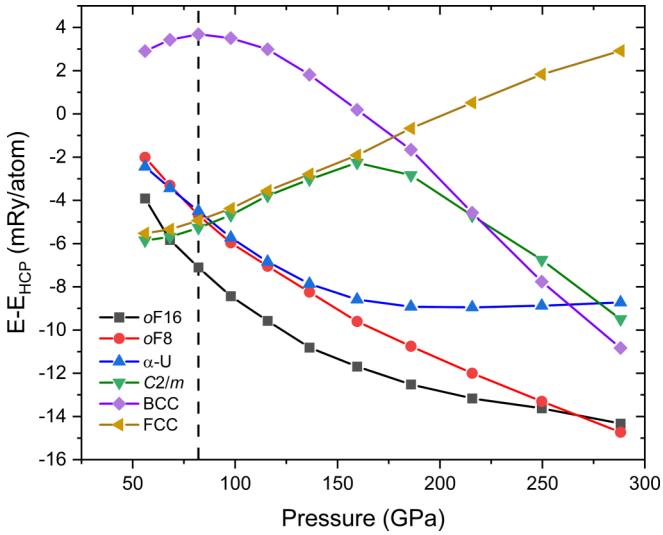

FIG. 7. Energy as a function of pressure relative to the hcp structure comparing a select few candidate structures for the collapsed phase of Dy. As the prevolume collapse phase *h*R24 is well established experimentally to pressures up to ∼80 GPa, this plot is focused on the potential structures of the volume collapsed phase and beyond. Pressure points below 80 GPa are only shown to better elucidate the trends of the various calculated phases. The dashed line shows the experimentally determined pressure for the volume collapse transition of ∼82 GPa. Above this transition, the *o*F16 structure is shown to be the more energetically favorable structure until ∼275 GPa, at which point the *o*F8 structure type becomes more energetically favorable. Interestingly, the bcc structure begins to rapidly approach crossing the *o*F8 structure type, suggesting that bcc may become the more energetically favorable structure for pressures greater than 375 GPa.

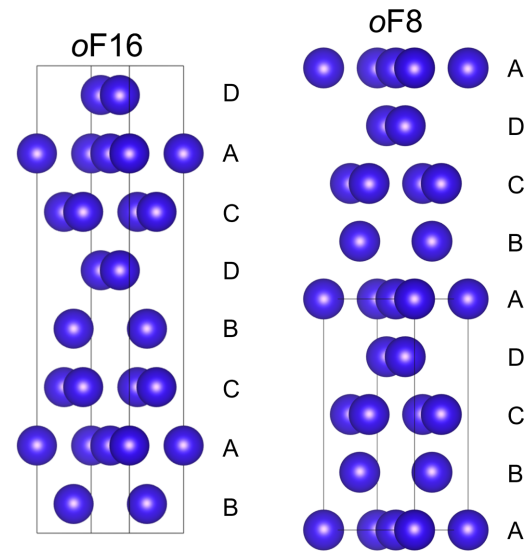

FIG. 8. Comparison of atomic stacking between *o*F16 and *o*F8 polytypes. Labeling has been shifted for the *o*F16 stacking sequence from the traditional ABCADCBD to correlate similar stacking planes between structures. Gray lines represent the unit cell of each structure.

steep and an extrapolation suggests it will become the more energetically favorable phase above 375 GPa. More detailed structure searches will need to be performed in the future to test other likely candidate structures.

IV. CONCLUSIONS

In conclusion, we have presented a detailed experimental study of Dy metal compressed in a soft pressure transmitting medium to a maximum pressure of 182 GPa coupled with theoretical calculations focused on the pressure region between 50 and 300 GPa. In our experimental data, we observe the previously reported structural transition sequence through the collapsed phase and measure starting transition pressures of 5.77(3) GPa for the hcp→α-Sm (*h*P2 → *h*R9) transition, 17.2(3) GPa for the α-Sm→dhcp (*h*R9 → *h*P4) transition, 37.2(9) GPa for the dhcp→dfcc (*h*P4 → *h*R24) transition, and 82.1(1.6) GPa for the volume collapse transition; and we report a 3.4(7)% change in volume between the *h*R24 and *o*F16 structures. Dy metal shows anisotropic compression behavior attributed to changes within the electron distribution which can be amplified by nonhydrostatic conditions. This complex behavior is most likely the source of the large variation in values reported in literature for both transition pressures and the magnitude of the volume collapse. This work shows the necessity of employing a soft pressure transmitting medium, even when compressing a "soft" material such as Dy. Furthermore, this is a study on Dy in which the high-pressure structural behavior of the collapsed phase seen in experimental data has been verified by theoretical calculations, as well as a study which has evaluated potential new structures at pressures beyond that which has been achieved experimentally. These calculations have predicted that Dy metal will undergo an isosymmetric phase transformation above 275 GPa in which the stacking configuration changes from eightfold stacking in the *o*F16 structure to fourfold stacking in the *o*F8 structure. Extrapolation of our calculations to even higher pressures indicates that Dy may transform to the bcc structure above 375 GPa, showing that there is still much to explore regarding the high-pressure behavior of Dy, as well as the other rare-earth metals. Further experiments utilizing toroidal anvils to access pressures above 300 GPa, as well as more detailed structure searches will be necessary to elucidate the behavior of these systems at extreme conditions.

ACKNOWLEDGMENTS

We thank E. Pace and M. McMahon for providing the lattice parameter and volumes for Y from their recent publication (Ref. [6]). This work was performed under the auspices of the U.S. Department of Energy by Lawrence Livermore National Laboratory under Contract No. DE-AC52-07NA27344. Portions of this work were performed at HPCAT (Sector 16), APS, Argonne National Laboratory. HPCAT operations are supported by DOE-NNSA's Office of Experimental Sciences. The Advanced Photon Source is a U.S. Department of Energy (DOE) Office of Science User Facility operated for the DOE Office of Science by Argonne National Laboratory under Contract No. DE-AC02-06CH11357.

[1] J. C. Duthie and D. G. Pettifor, Correlation between d-Band Occupancy and Crystal Structure in the Rare Earths, Phys. Rev. Lett. **38**, 564 (1977).

[2] B. Johansson, Structural and electronic relationships between the lanthanide and actinide elements, Hyperfine Interact. **128**, 41 (2000).

[3] J. Akella, G. S. Smith, and S. T. Weir, Static ultra-high pressure study of lanthanide and actinide metals using a diamond-anvil cell, AIP Conf. Proc. **309**, 187 (1994).

[4] M. I. McMahon, S. Finnegan, R. J. Husband, K. A. Munro, E. Plekhanov, N. Bonini, C. Weber, M. Hanfland, U. Schwarz, and S. G. Macleod, Structure and magnetism of collapsed lanthanide elements, Phys. Rev. B **100**, 024107 (2019).

[5] G. Fabbris, T. Matsuoka, J. Lim, J. R. L. Mardegan, K. Shimizu, D. Haskel, and J. S. Schilling, Different routes to pressure-induced volume collapse transitions in gadolinium and terbium metals, Phys. Rev. B **88**, 245103 (2013).

[6] E. J. Pace, S. E. Finnegan, C. V. Storm, M. Stevenson, M. I. McMahon, S. G. MacLeod, E. Plekhanov, N. Bonini, and C. Weber, Structural phase transitions in yttrium up to 183 GPa, Phys. Rev. B **102**, 094104 (2020).

[7] Y. K. Vohra and S. L. Beaver, Ultrapressure equation of state of cerium metal to 208 GPa, J. Appl. Phys. **85**, 2451 (1999).

[8] G. N. Chesnut and Y. K. Vohra, Phase transformations and equation of state of praseodymium metal to 103 GPa, Phys. Rev. B **62**, 2965 (2000).

[9] S. E. Finnegan, C. V. Storm, E. J. Pace, M. I. McMahon, S. G. MacLeod, E. Plekhanov, N. Bonini, and C. Weber, High-pressure structural systematics in neodymium up to 302 GPa, Phys. Rev. B **103**, 134117 (2021).

[10] J. Lim, G. Fabbris, D. Haskel, and J. S. Schilling, Record high magnetic ordering temperature in a lanthanide at extreme pressure, J. Phys.: Conf. Ser. **950**, 042025 (2017).

[11] J. Lim, G. Fabbris, D. Haskel, and J. S. Schilling, Origin of the volume collapse under pressure in elemental Dy, J. Phys.: Conf. Ser. **500**, 192009 (2014).

[12] R. Patterson, C. K. Saw, and J. Akella, Static high-pressure structural studies on Dy to 119 GPa, J. Appl. Phys. **95**, 5443 (2004).

[13] G. Fabbris, J. Lim, L. S. I. Veiga, D. Haskel, and J. S. Schilling, Electronic and structural ground state of heavy alkali metals at high pressure, Phys. Rev. B **91**, 085111 (2015).

[14] S. E. Finnegan, E. J. Pace, C. V. Storm, M. I. McMahon, S. G. MacLeod, H. P. Liermann, and K. Glazyrin, High-pressure structural systematics in samarium up to 222 GPa, Phys. Rev. B **101**, 174109 (2020).

[15] N. C. Cunningham, W. Qiu, K. M. Hope, H.-P. Liermann, and Y. K. Vohra, Symmetry lowering under high pressure: Structural evidence for f-shell delocalization in heavy rare earth metal terbium, Phys. Rev. B **76**, 212101 (2007).

[16] Y. R. Shen, R. S. Kumar, A. L. Cornelius, and M. F. Nicol, High-pressure structural studies of dysprosium using angle-dispersive x-ray diffraction, Phys. Rev. B **75**, 064109 (2007).

[17] O. Tschauner, O. Grubor-Urosevic, P. Dera, and S. R. Mulcahy, Anomalous elastic behavior in hcp- and Sm-type dysprosium, J. Phys. Chem. C **116**, 2090 (2011).

[18] K. M. Hope, C. S. Perreault, and Y. K. Vohra, High pressure structural phase transitions in dysprosium to 202 GPa, High Pressure Res. **42**, 47 (2022).

[19] G. K. Samudrala and Y. K. Vohra, Crystallographic phases in heavy rare earth metals under megabar pressures, J. Phys.: Conf. Ser. **377**, 012111 (2012).

[20] K. Takemura, Hydrostaticity in high pressure experiments: Some general observations and guidelines for high pressure experimenters, High Pressure Res. **41**, 155 (2021).

[21] E. F. O'Bannon, P. Söderlind, D. Sneed, M. J. Lipp, H. Cynn, J. S. Smith, C. Park, and Z. Jenei, High pressure stability of β-Zr: No evidence for isostructural phase transitions, High Pressure Res. **41**, 247 (2021).

[22] Z. Jenei, H. Cynn, K. Visbeck, and W. J. Evans, High-temperature experiments using a resistively heated high-pressure membrane diamond anvil cell, Rev. Sci. Instrum. **84**, 095114 (2013).

[23] A. Dewaele, M. Torrent, P. Loubeyre, and M. Mezouar, Compression curves of transition metals in the mbar range: Experiments and projector augmented-wave calculations, Phys. Rev. B **78**, 104102 (2008).

[24] See Supplemental Material at http://link.aps.org/supplemental/10.1103/PhysRevB.105.214110 for details associated with the ambient structure refinement, details on lattice parameters as a function of pressure, comparison to previous datasets, comparisons between refinement and peak fitting values for the collapsed phase, equation of state details, discussions on uncertainties, and tables of experimental and calculated data, which includes Ref. [44].

[25] J. S. Smith, E. A. Rod, and G. Shen, Fly scan apparatus for high pressure research using diamond anvil cells, Rev. Sci. Instrum. **90**, 015116 (2019).

[26] C. Prescher and V. B. Prakapenka, DIOPTAS: A program for reduction of two-dimensional X-ray diffraction data and data exploration, High Pressure Res. **35**, 223 (2015).

[27] B. H. Toby and R. B. Von Dreele, GSAS-II: The genesis of a modern open-source all purpose crystallography software package, J. Appl. Crystallogr. **46**, 544 (2013).

[28] A. Dewaele, P. Loubeyre, and M. Mezouar, Equations of state of six metals above 94 GPa, Phys. Rev. B **70**, 094112 (2004).

[29] A. Dewaele, F. Datchi, P. Loubeyre, and M. Mezouar, High pressure–high temperature equations of state of neon and diamond, Phys. Rev. B **77**, 094106 (2008).

[30] J. Gonzalez-Platas, M. Alvaro, F. Nestola, and R. Angel, EosFit7-GUI: A new graphical user interface for equation of state calculations, analyses and teaching, J. Appl. Cryst. **49**, 1377 (2016).

[31] P. Söderlind and D. Young, Assessing density-functional theory for equation-of-state, Computation **6**, 13 (2018).

[32] Y.-C. Wang, B.-L. Liu, Y. Liu, H.-F. Liu, Y. Bi, X.-Y. Gao, J. Sheng, H.-Z. Song, M.-F. Tian, and H.-F. Song, The underestimation of high pressure in DFT+U simulation for the wide range cold-pressure of lanthanide metals, arXiv:2111.12863.

[33] P. Söderlind, P. E. A. Turchi, A. Landa, and V. Lordi, Ground-state properties of rare-earth metals: An evaluation of density-functional theory, J. Phys.: Condens. Matter **26**, 416001 (2014).

[34] P. Söderlind, Delocalization and phase transitions in Pr: Theory, Phys. Rev. B **65**, 115105 (2002).

[35] J. M. Wills, M. Alouani, P. Andersson, A. Delin, O. Eriksson, and O. Grechnyev, *Full-Potential Electronic Structure Method: Energy and Force Calculations with Density Functional and*

Dynamical Mean Field Theory, Springer Series in Solid-State Sciences Vol. 167 (Springer, New York, 2010).

[36] F. Birch, Equation of state and thermodynamic parameters of NaCl to 300 kbar in the high-temperature domain, J. Geophys. Res.: Solid Earth **91**, 4949 (1986).

[37] O. L. Anderson, in *Equations of State of Solids for Geophysics and Ceramic Science*, Oxford Monographs on Geology and Geophysics Vol. 31 (Oxford University Press, Oxford, 1995), p. 377.

[38] W. A. Grosshans and W. B. Holzapfel, On structural systematics of the lanthanides under pressure, J. Phys. Colloques **45**, C8-141 (1984).

[39] N. Hamaya, Y. Sakamoto, H. Fujihisa, Y. Fujii, K. Takemura, T. Kikegawa, and O. Shimomura, Crystal structure of the distorted FCC high-pressure phase of praseodymium, J. Phys.: Condens. Matter **5**, L369 (1993).

[40] S. Heathman, R. G. Haire, T. L. Bihan, A. Lindbaum, K. Litfin, Y. Meresse, and H. Libotte, Pressure Induces Major Changes in the Nature of Amercium's 5f Electrons, Phys. Rev. Lett. **85**, 2961 (2000).

[41] S. Heathman, T. Le Bihan, S. Yagoubi, B. Johansson, and R. Ahuja, A high-pressure structure in curium linked to magnetism, Science **309**, 110 (2005).

[42] S. Heathman, T. Le Bihan, S. Yagoubi, B. Johansson, and R. Ahuja, Structural investigation of californium under pressure, Phys. Rev. B **87**, 214111 (2013).

[43] P. Söderlind, First-principles phase stability, bonding, and electronic structure of actinide metals, J. Electron Spectrosc. Relat. Phenom. **194**, 2 (2014).

[44] W. J. Carter, J. N. Fritz, S. P. Marsh, and R. G. McQueen, Hugoniot equation of state of the lanthanides, J. Phys. Chem. Solids **36**, 741 (1994).